TOPICAL REVIEW • OPEN ACCESS

Anisotropy-driven topological quantum phase transition in magnetic impurities

IOP Publishing Mater. Quantum Technol. 4 (2024) 042001 https://doi.org/10.1088/2633-4356/ada081

Materials for Quantum Technology

OPEN ACCESS

RECEIVED
29 December 2023

REVISED
5 December 2024

ACCEPTED FOR PUBLICATION
17 December 2024

PUBLISHED
27 December 2024

TOPICAL REVIEW

Anisotropy-driven topological quantum phase transition in magnetic impurities

G G Blesio[1], L O Manuel[1,*] and A A Aligia[2]

[1] Instituto de Física de Rosario (CONICET) and Facultad de Ciencias Exactas, Ingeniería y Agrimensura, Universidad Nacional de Rosario, Rosario, Argentina
[2] Instituto de Nanociencia y Nanotecnología CNEA-CONICET, GAIDI, Centro Atómico Bariloche and Instituto Balseiro, 8400 Bariloche, Argentina
[*] Author to whom any correspondence should be addressed.

E-mail: manuel@ifir-conicet.gov.ar

Keywords: topological quantum phase transition, scanning-tunneling spectroscopy, Kondo physics, NRG

Abstract

A few years ago, a topological quantum phase transition (TQPT) has been found in Anderson and Kondo 2-channel spin-1 impurity models that include a hard-axis anisotropy term DS_z^2 with $D > 0$. The most remarkable manifestation of the TQPT is a jump in the spectral density of localized electrons, at the Fermi level, from very high to very low values as D is increased. If the two conduction channels are equivalent, the transition takes place at the critical anisotropy $D_c \sim 2.5\ T_K$, where T_K is the Kondo temperature for $D = 0$. This jump might be important to develop a molecular transistor. The jump is due to a corresponding one in the Luttinger integral, which has a topological non-trivial value $\pi/2$ for $D > D_c$. Here, we review the main results for the spectral density and highlight the significance of the theory for the interpretation of measurements conducted on magnetic atoms or molecules on metallic surfaces. In these experiments, where D is held constant, the energy scale T_K is manipulated by some parameters. The resulting variation gives rise to a differential conductance $\mathrm{d}I/\mathrm{d}V$, measured by scanning-tunneling spectroscopy, which is consistent with a TQPT at an intermediate value of T_K. For non-equivalent channels and non-zero magnetic field, the topological phase is lost but still a peculiar behaviour in the spectral density is obtained which agrees with experimental observations. We also show that the theory can be extended to integer spin $S > 1$ and two-impurity systems. This is also probably true for half-integer spin and non-equivalent channels in some cases.

1. Introduction

Systems with individual magnetic atoms [1] or molecules [2–6] on metallic surfaces are being studied extensively in the last years due to their peculiar properties and potential application in spintronics and molecular electronics. A fundamental component within an integrated circuit is the transistor, which can be realized in these magnetic impurity systems through the controlled switching of the electric current by varying some physical parameters [4].

A realistic analysis of magnetic impurity systems requires taking into account their potential multiorbital nature and hybridization with more than one conduction channel. Indeed, a plethora of electronic states, ranging from Landau-Fermi liquid to singular Fermi liquid and non-Fermi liquid, emerges depending on the specific value of the spin of the magnetic impurity and the number of conduction channels [7]. An important, although often overlooked, physical ingredient of multiorbital systems is the single-ion magnetic anisotropy DS_z^2 due to the spin–orbit coupling (SOC), enhanced in the low-symmetry arrangements of atoms or molecules on surfaces.

As an example of the relevance of single-ion anisotropy, some years ago, it has been found that the conductance of a system composed of a Ni impurity in a Au chain doped with oxygen has a jump as a function of the anisotropy D of the spin 1 of the Ni atom, suggesting that the system could act as a

transistor [8, 9]. The underlying model is the 2-channel spin-1 Anderson model with anisotropy (2CS1AMA) or its integer valent limit, the anisotropic two-channel spin-1 Kondo model (A2CS1KM). Both models are described in section 2. With such models, it can be seen that the jump is due to a local topological quantum phase transition (TQPT) between two phases that differ in the value of the so-called Luttinger integral I_L, whose zero value had been for decades a hallmark of a Fermi liquid [10]. For low D/T_K where T_K is the Kondo temperature for $D=0$, the system is in the topologically trivial phase with $I_L=0$, characterized by a large spectral density of localized electrons at the Fermi level and large conductance at low temperatures and bias voltage. For large D/T_K the system is topologically non-trivial with $I_L=\pi/2$, with a pronounced dip in the conductance and spectral density of localized electrons at low energies. This phase has been called 'non-Landau' Fermi liquid, because it cannot be adiabatically connected to a non-interacting system for which $I_L=0$ [8, 10].

For degenerated channels and zero magnetic field $B=0$, the transition takes place at the critical anisotropy $D_c\sim 2.5\ T_K$. However, the TQPT still exists for $B\neq 0$ or inequivalent channels with $B=0$ [11]. For non-equivalent channels and $B\neq 0$, the system is a topologically trivial conventional Fermi liquid, but a crossover from a dip to a peak can be induced by modifying a parameter like B [11] and has been actually observed, as explained in section 6.1.

Previous studies have identified a variety of local QPTs in impurity systems. Among the most notable are the transition from the conventional Kondo state to the non-Fermi liquid state in two-channel Kondo systems and the Kondo to local moment transition in the pseudogap Kondo model (see, for example, [12–14] and references therein). However, the nature of our transition is different. In our case, the transition takes place between two topologically different Fermi liquids [8, 11], characterized by different Luttinger integrals I_L –which can be reexpressed as a topological winding number [8]– implying necessarily that one of these liquids cannot be adiabatically connected to a non-interacting system. This liquid has been called a topological or a 'non-Landau' one to distinguish it from a conventional Fermi liquid. Similar QPTs to ours have also been observed in two-impurity systems, where each impurity is coupled to its own conduction band, and the two impurities interact through both an antiferromagnetic exchange interaction and a direct Coulomb interaction [15, 16].

In two-channel spin-1/2 models there is a QPT from a Fermi liquid to a non-Fermi liquid [12], whose Luttinger integral can take a continuous set of values, depending on the occupation of the impurity [17]. In the pseudogap case [13], the transition takes place between a conventional Fermi liquid and a local moment phase, consisting in a Fermi liquid with an uncoupled spin 1/2. In the one-channel singlet-triplet models (which hybridizes a configuration with a singlet and a triplet with another one with a doublet) [18–21], the QPT separates a conventional Fermi liquid and a singular Fermi liquid, characterized by a non-analytical low frequency self-energy, proper of an underscreened Kondo effect. The singular Fermi liquid is characterized by a discrete non-zero I_L [17, 19, 22, 23]. However, as for non-Fermi liquids, the Friedel–Langreth sum rules discussed in section 3 are not expected to apply. A spin $S=3/2$ with anisotropy D interacting with two conduction channels undergoes a QPT at $D=0$ where a system is a singular Fermi liquid. This critical point separates a Fermi liquid phase with a decoupled spin for $D<0$ and a non-Fermi liquid phase for $D>0$ [24, 25].

In this article, we review the main results concerning the above mentioned local TQPT. While the original model was proposed for a particular system that has not been realized up to date [26], we show that several systems with magnetic atoms or molecules on metallic surfaces can be actually described by the 2CS1AMA, or the simpler A2CS1KM, providing a consistent and unified description of several experiments. Alternatives theories, sometimes inconsistent between them or physically unjustified, have been proposed to interpret the outcome of those experiments. This is probably due to the fact that the theory is rather recent, and that to describe the TQPT, a very accurate technique like the numerical renormalization group (NRG) is required, which is computationally expensive for two or more channels. So far, no other technique has been able to capture the TQPT. We also show that the theory can be extended to a larger spin and two-impurity systems.

The paper is organized as follows. In section 2 we introduce the two models, Kondo and Anderson, for the spin-1 impurity coupled with two conduction channels. In section 3 the NRG predictions for the localized electron spectral density are presented and discussed in the context of the TQPT. In section 4 we show that the models we studied can be mapped onto those of two $S=1/2$ impurities coupled through an (in general anisotropic) exchange interaction between them. In section 5 the theory is generalized for $S>1$. In section 6, the differential conductance ($\mathrm{d}I/\mathrm{d}V$) measurements for five different systems are discussed and compared with the theoretical calculations for $S=1$: 6.1) FePc on Au(111), 6.2) MnPc on Au(111), 6.3) nickelocene on Cu(100), 6.4) Fe atoms on MoS_2/Au(111) and 6.5) Fe porphyrin molecules on Au(111). Finally, we conclude with a brief summary in section 7.

2. Models

The simplest model to describe the local TQPT is the A2CS1KM. It takes the form

$$H_{\rm K} = \sum_{k\tau\sigma} \varepsilon_{k\tau} c^\dagger_{k\tau\sigma} c_{k\tau\sigma} + \sum_{k\tau\sigma\sigma'} \frac{J^\tau_{\rm K}}{2} c^\dagger_{k\tau\sigma} \vec{\sigma}_{\sigma\sigma'} c_{k\tau\sigma'} \cdot \vec{S} + DS_z^2 - BS_z, \tag{1}$$

where $c^\dagger_{k\tau\sigma}$ creates a conduction electron with point-group symmetry $\tau = \pm 1$ (channel index), spin σ and remaining quantum numbers k. The first term describes the substrate conduction bands, the second term is the Kondo exchange interaction between conduction electrons and the localized spin $\vec{S}$ with exchange couplings $J^\tau_{\rm K}$, DS_z^2 is the single-ion uniaxial magnetic anisotropy, B is the magnetic field and $\vec{\sigma}$ is the vector of Pauli matrices. The simplest case is when the two channels are equivalent: both are degenerate ($\varepsilon_{k\tau} = \varepsilon_k$) and the localized spin is equally coupled to them ($J^\tau_{\rm K} = J_{\rm K}$).

When intermediate valence of the magnetic impurity is included, the model is the 2-channel spin-1 Anderson model with anisotropy (2CS1AMA). It can be written in the form used first for Ni compounds with holes in the xz and yz orbitals [9, 27, 28]. Extension to other cases, for example, FePc on Au(111) [11] are straightforward. Neglecting the pair-hopping term [9], which is irrelevant in all cases considered so far as the intra-orbital Coulomb U repulsion is considerably larger that the inter-orbital U' one, the Anderson Hamiltonian is

$$\begin{aligned} H = &\sum_{k\tau\sigma} \varepsilon_k c^\dagger_{k\tau\sigma} c_{k\tau\sigma} + \sum_{k\tau\sigma} \left(v_\tau c^\dagger_{k\tau\sigma} d_{\tau\sigma} + \text{H.c.} \right) \\ &+ \sum_{\tau\sigma} \epsilon d^\dagger_{\tau\sigma} d_{\tau\sigma} + \sum_{\tau} U n_{\tau\uparrow} n_{\tau\downarrow} + U' n_{xz} n_{yz} - J_H \vec{S}_{xz} \cdot \vec{S}_{yz} + DS_z^2 - BS_z, \end{aligned} \tag{2}$$

where $d^\dagger_{\tau\sigma}$ ($c^\dagger_{k\tau\sigma}$) creates a hole with energy ϵ (ε_k) in the d orbital τ (conduction band τ with momentum k), with $\tau = xz, yz$. $n_{\tau\sigma} = d^\dagger_{\tau\sigma} d_{\tau\sigma}$ and $n_\tau = \sum_\sigma n_{\tau\sigma}$. v_τ is the tunneling or hybridization amplitude between impurity and conduction states (assumed to be independent of k), while $J_{\rm H}$ is the strong Hund ferromagnetic exchange between the spins $\vec{S}_\tau$ of both orbitals responsible for the total spin $\vec{S} = \vec{S}_{xz} + \vec{S}_{yz}$ one of the impurity. The projection of $\vec{S}$ in the direction of anisotropy is denoted as S_z.

For small hybridization and when the two-particle configuration dominates, the model (2) reduces to the A2CS1KM [9].

3. Main properties of the two-channel spin-1 models

3.1. Two equivalent channels at zero magnetic field

In the simplest case, without spin or channel anisotropy ($B = 0$, $J^\tau_{\rm K} = J_{\rm K}$ independent of τ), it has been found that the TQPT in the A2CS1KM occurs at an anisotropy $D_{\rm c} \sim 2.5\ T_{\rm K}$, where $T_{\rm K}$ is the Kondo temperature for $D = 0$ [9]. The evolution of the spectral density for localized states $\rho(\omega)$ with D for constant $T_{\rm K}$ is shown in figure 11 of [9], where an abrupt change at the Fermi level signals the critical value $D_{\rm c}$

In figure 1 we represent $\rho(\omega)$ for different Kondo exchange couplings $J_{\rm K}$, keeping $D = 0.0027\ W$ constant, where W is the half-bandwidth of the conduction bands, taken as the energy unit. $r \equiv J_{\rm K}/J_{\rm Kc}$, where $J_{\rm Kc}$ is the critical Kondo coupling for the given D ($J_{\rm K}$ such that $D \simeq 2.5\ T_{\rm K}$). The numerical calculations were performed with the Ljubljana code of the NRG [29, 30]. We assume flat conduction bands extending from $-W$ to W for both symmetries.

For r significantly larger than 1, the spectral density of localized states is similar to that of a conventional Kondo peak. For r slightly larger than 1, $\rho(\omega)$ has the form of a narrow peak mounted on a broad peak. The latter, at the Fermi level, has around half the magnitude expected for the usual compensated Kondo model and therefore, it is similar to the spectral density expected for the spin-1/2 two-channel Kondo model (2CKM). However, as long as $r > 1$, the system satisfies the conventional Friedel–Langreth sum rule (the small deviation in the figure is due to numerical errors of the NRG) and $\rho(0)$ has its maximum possible value. However, as soon as $r < 1$, $\rho(0)$ jumps to 0. This is due to a jump in the Luttinger integral from 0 to $\pi/2$ at $r = 1$ [8, 11], as discussed below. If r is decreased further, the shape of the spectral density tends to be rectangular, with two jumps at $-D$ and D, typical of inelastic scattering when only one channel is present [31–34]. These steps are overbroadened in figure 1 due to technical reasons that limit the resolution of the NRG at large energies [35].

A detailed description of what happens with the Friedel–Langreth sum rule and the Luttinger integrals in the more general case, which includes intermediate valence, different channels, and a magnetic field has been explained in detail in the supplemental material of [11]. To avoid including many technical details, we

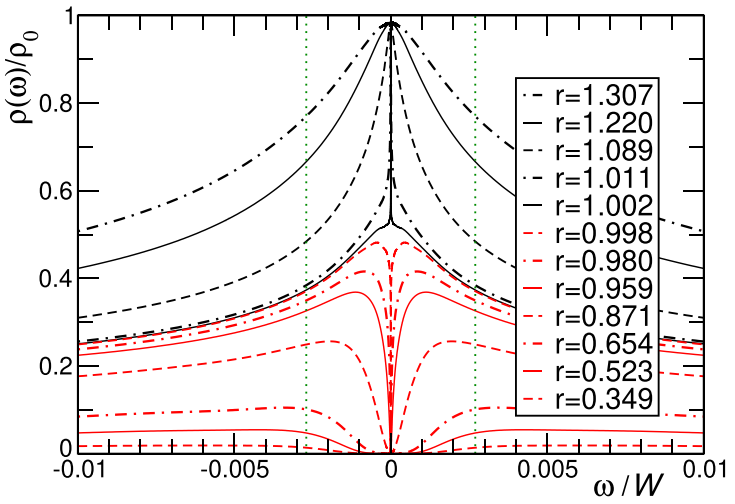

Figure 1. Spectral density of localized electrons of the A2CS1KM as a function of energy for several values of $r = J_K/J_{Kc}$, where J_{Kc} is the value of J_K at the TQPT. ρ_0 is given by the conventional Friedel sum rule with vanishing Luttinger integral [11]. Vertical dotted lines are at $\omega = \pm D$. $\omega = 0$ corresponds to the Fermi level.

outline the main facts for the simpler case of equivalent conduction channels and zero magnetic field in the two-orbital Anderson model, for which the Luttinger integral I_L does not depend on the spin and channel quantum numbers.

Using conservation laws, it can be shown that the spectral function of the localized states for each orbital and spin, at the Fermi level and $T = 0$, is given by

$$\rho_{\tau\sigma}(\omega = 0) = \frac{1}{\pi \Delta_\tau} \sin^2(\delta_{\tau\sigma}), \tag{3}$$

where $\Delta_\tau = \pi v_\tau^2 \rho_c$, with ρ_c the density of conduction states assumed independent of energy. The phase shift suffered by the conduction electrons at the Fermi level due to the presence of the impurity is

$$\delta_{\tau\sigma} = \pi \langle n_{\tau\sigma} \rangle - I_L^{\tau\sigma}. \tag{4}$$

The Luttinger integral I_L (independent of orbital and spin indices in the simplest case) is defined as

$$I_L^{\tau\sigma} = \mathrm{Im} \int_{-\infty}^{0} d\omega G_{\tau\sigma}^d(\omega) \frac{\partial \Sigma_{\tau\sigma}^d(\omega)}{\partial \omega}, \tag{5}$$

where $G_{\tau\sigma}^d(\omega)$ is the impurity Green function for orbital τ and spin σ, and $\Sigma_{\tau\sigma}^d(\omega)$ is the corresponding self energy.

For a long time, I_L has been assumed to vanish for a Fermi liquid, based on perturbation calculations starting from a non-interacting electronic system [10, 36, 37]. However, rather recently [15, 16] it has been found that this is not always the case for local Fermi liquids. A topological interpretation of I_L was provided for extended systems in [38] and extended to the impurity case in [8]. Specifically, defining the ratio of non-interacting and interacting Green functions

$$D_{\tau\sigma}(z) = \frac{G_{\tau\sigma}^{d(0)}(z)}{G_{\tau\sigma}^d(z)}, \tag{6}$$

it has been shown that $I_L^{\tau\sigma}$ is given by the sum of the winding number of $D_{\tau\sigma}(z)$ around a circuit that surrounds the negative frequency axis plus half the corresponding winding number for a circuit that surrounds the origin (see the supplemental material of [8] and [11]).

An explicit calculation has shown that in the 'non-Landau' phase, for large D/T_K, $I_L^{\tau\sigma} = \pi/2$ [11]. In the Kondo limit, $\langle n_{\tau\sigma} \rangle = 1/2$ and equation (3) gives $\rho_{\tau\sigma}(0) = 0$ in this phase, whereas in the conventional Fermi liquid phase, with $I_L = 0$, the spectral density at the Fermi level has its maximum possible value $\rho_{\tau\sigma}(0) = 1/(\pi\Delta)$. This explains the jump observed in figure 1 at the TQPT.

Previously a non-trivial value of I_L has been found in underscreened one-channel spin-1 models, for which the system is a singular Fermi liquid [19].

We note that simpler alternative approaches to NRG fail to capture the QPT. While the non-crossing approximation can describe non-Fermi liquid behavior quite well [25] it does not capture correctly the 'non-Landau' phase [9] or in general phases where the isolated impurity has a non-degenerate ground state [20]). The slave-boson mean-field approximation [39] reduces the system to a non-interacting one, thus always resulting in a conventional Fermi liquid. For single-channel systems, perturbation theory up to third order in the exchange interaction J_K has successfully explained certain experiments involving spins $S > 1/2$ for $D \gg T_K$ [40]. However, it becomes unreliable for larger T_K, and extending this approach to two-channel systems is cumbersome.

In [8], the conductance through a two-channel spin-1 impurity was calculated using the Anderson Hamiltonian equation (2). Curiously at the quantum critical point and in a more extended critical region at finite temperatures, the spectral density and the conductance resemble those of a spin-1/2 2CKM, which is a non-Fermi liquid. The value of the conductance at zero voltage and that of the spectral density at zero frequency are both half those expected in the Kondo regime for a conventional Fermi liquid. This is further confirmed by an analysis of the eigenvalues from the NRG flow, which we briefly comment on below. For more detailed information, interested readers can refer to the supplemental material in [8].

Increasing the length of the Wilson chain N corresponds to lower temperatures. For values of the anisotropy D close to the critical one D_c and small N, the system is in the regime of the spin-1/2 2CKM. The NRG energy flow exhibits an extended plateau, without even–odd alternation in the eigenvalues, signaling the existence of an unstable fixed point at intermediate temperatures. For larger N (smaller temperatures), the system enters in the regime of one of the Fermi liquids depending on the sign of $D - D_c$ (topological for positive $D - D_c$). The flow is typical of the Fermi liquid, with even–odd alternation. At the large N fixed points there is a simple relation between the eigenvalues of both cases: $E_{N+1}(D > D_c) = E_N(D < D_c)$. This can be understood considering that, in the strong-coupling fixed point and for $D > D_c$ the impurity is decoupled, while for $D < D_c$ it is strongly coupled to the first site of the conduction chain, effectively removing it from the non-interacting chain.

Increasing the length of the Wilson chain N corresponds to lower temperatures. For values of the anisotropy D close to the critical value D_c and small N, the system is in the regime of the spin-1/2 2CKM. The NRG energy flow exhibits an extended plateau, with no even–odd alternation in the eigenvalues, indicating the presence of an unstable fixed point at intermediate temperatures. For larger N (or lower temperatures), the system enters the regime of one of the Fermi liquids, depending on the sign of $D - D_c$ (topological for $D - D_c > 0$). The flow is characteristic of a Fermi liquid, with even–odd alternation. At the large N fixed points, there is a simple relationship between the eigenvalues of the two cases: $E_{N+1}(D > D_c) = E_N(D < D_c)$. This can be understood by noting that, at the strong-coupling fixed point, for $D > D_c$, the impurity is decoupled, while for $D < D_c$, it is strongly coupled to the first site of the conduction chain, effectively removing it from the non-interacting chain.

3.2. Effect of channel anisotropy

As stated above, for equivalent channels ($J_K^{-1} = J_K^l$) the critical value of D at the transition is $D_c \sim 2.5\ T_K$. From results with only one channel [33, 34] one knows that $D_c \to 0$ for $J_K^{-1} \to 0$.

We define the Kondo temperature $T_K^{(\tau)}$ as the temperature for which the contribution of channel τ to the zero-bias conductance for $D = B = 0$ falls to half of its zero-temperature value [8].

Clearly, the ratio $D_c/T_K^{(1)}$ should decrease as the coupling ratio J_K^{-1}/J_K^l decreases. In figure 2 we display the relation between both quantities near $J_K^{-1}/J_K^l = 0.5$ which appears to be relevant ratio for iron phthalocyanine on Au(111) (see section 6.1). Decreasing J_K^{-1}/J_K^l from 1 to 0.5, $D_c/T_K^{(1)}$ has decreased by an order of magnitude, making it feasible to reach the 'non-Landau' phase in the system with a moderate anisotropy. We note that the highest Kondo temperature $T_K^{(1)}$ increases slightly with decreasing J_K^{-1} ($T_K^{(1)} \sim 0.021 \pm 0.03$ in the range of the figure). Instead, T_K^{-1} decreases strongly [11].

3.3. Effect of magnetic field with channel anisotropy

The strong decrease in D_c with channel anisotropy makes it experimentally feasible to observe the effects of a magnetic field at moderate intensities, as we will discuss in section 6.

However, the inclusion of a magnetic field complicates the theory, as it breaks both spin and channel symmetries. When channels and spins are equivalent, equations (3) and (4) are derived using a single conservation law. If one of these symmetries is broken, there are two conservation laws, corresponding to two independent Luttinger integrals $I_L^{\tau\sigma}$ [see equation (5)]. When both symmetries are broken one has three conservation laws (for total number of particles, spin and channel pseudospin) leading for three topological numbers for four Luttinger integrals. A detailed analysis (see supplemental material of [11]) shows that as soon as a non-zero magnetic field B is introduced, the Luttinger integrals lose their topological nature and

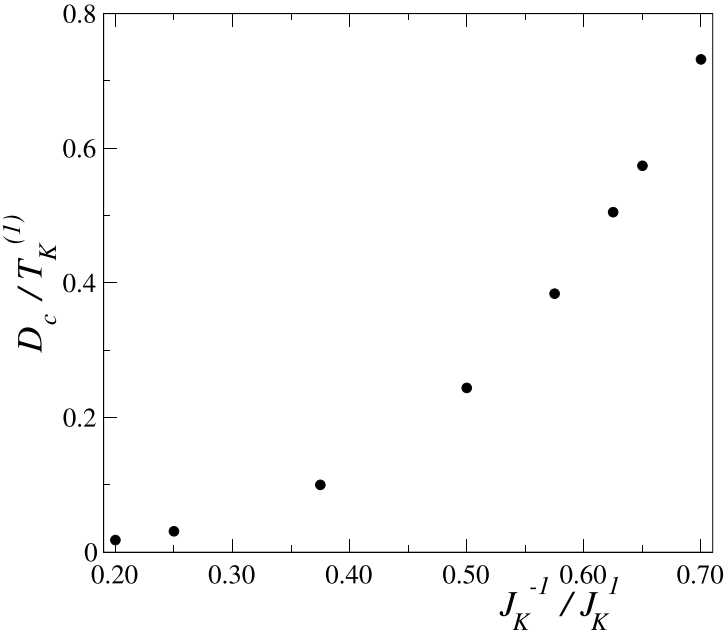

Figure 2. Ratio of the critical anisotropy D_c over the higher Kondo temperature, varying the smaller exchange coupling J_K^{-1} with constant larger coupling $J_K^1 = 0.4$.

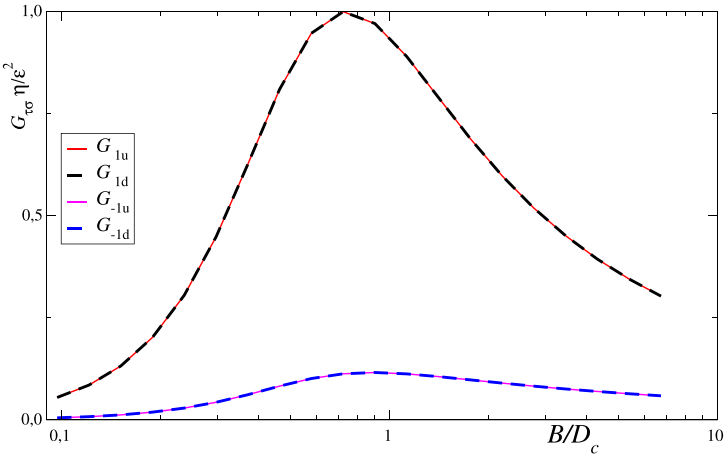

Figure 3. Contribution to the conductance for each channel and spin in the Anderson model as a function of magnetic field for $D/D_c = 1.67$.

become continuous variables. Therefore the system becomes a conventional Fermi liquid. However, all physical properties are continuous, in particular the conductance.

In figure 3 we show the contribution to the conductance at zero temperature for each channel and spin $G_{\tau\sigma}$ of the Anderson model equation (2) for parameters $U = 0.4$, $U' = 0$. $\epsilon = -U/2$, $J_H = 0.1$, $\Delta_1 = 0.06$, and $\Delta_{-1} = 0.0345$. Since these quantities are related with the corresponding phase shifts

$$G_{\tau\sigma}(\omega = 0) = \frac{e^2}{h}\sin^2(\delta_{\tau\sigma}), \tag{7}$$

they also give information of the spectral densities at the Fermi level [see equation (3)].

For small B, all $G_{\tau\sigma}$ are very small, as expected from the proximity of the system to the 'non-Landau' phase for $B = 0$ and $D > D_c$. As the magnetic field increases, the contributions of the more strongly coupled channel $G_{1\sigma}$, which are the same for both spins, increase and for $B \sim 0.7D_c$ they reach the maximum value, characteristic of the conventional Fermi liquid. For larger magnetic field $G_{1\sigma}$ decrease. This is also expected in the conventional Kondo regime, because the Kondo peak splits between spins up and down as B becomes larger than the Kondo temperature $T_K^{(1)}$.

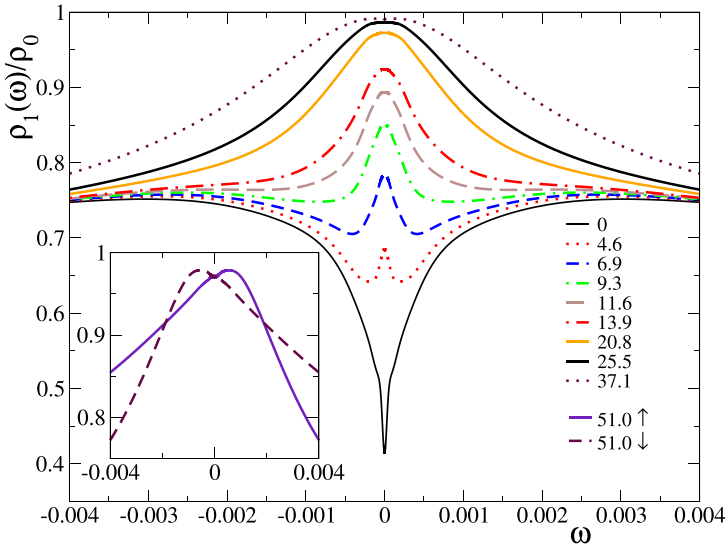

Figure 4. Spectral density of localized electrons of channel 1 in the A2CS1KM as a function of energy for several values of magnetic field in units of 10^{-4} for $J_K^{\perp} = 0.44$, $J_K^{-1} = 0.22$, and $D = 0.01$. Inset: spectral density resolved in spin, showing the splitting of the Kondo resonance for a large magnetic field.

In contrast, the contributions of the more weakly coupled channels $G_{-1\sigma}$ remain very small, although qualitatively the dependence with magnetic field is similar.

In figure 4 we represent the spectral density $\rho_1(\omega) = \rho_{1\uparrow}(\omega) + \rho_{1\downarrow}(\omega)$ of channel 1 (the most strongly coupled to the conduction band) as a function of magnetic field for parameters which correspond to the previous Anderson model through a Schrieffer–Wolf transformation, and an anisotropy slightly larger than the critical one $D_c = 0.0095$. Therefore, for $B = 0$, $\rho_{1\sigma}(\omega)$ has a narrow dip of width $\sim 10^{-3}$ similar to those displayed in figure 1 for D slightly larger than D_c. However while in that case, increasing the exchange couplings leads to an abrupt TQPT, in the present case, the spectral density changes continuously. For a magnetic field of the order of the width of the dip at $B = 0$, the dip disappears and leaves its place to a narrow peak that broadens. For larger magnetic fields, the splitting of the peaks for both spins begin to be important and the total spectral density at the Fermi level $\omega = 0$ decreases again. Note that $T_K^{(1)} \sim 0.034$ and thus, a complete splitting requires larger fields. This situation is similar to that observed in Mn phthalocyanine (see section 6.2).

4. Equivalence with two-impurity systems

In this section we that the two-channel spin-1 Anderson model with single-ion anisotropy [equation (2)] can be exactly mapped to a system of two $S = 1/2$ impurities coupled through an anisotropic exchange interaction between them. The Hamiltonian is

$$H_{2I} = \sum_{k\alpha\sigma} \varepsilon_k c^{\dagger}_{k\alpha\sigma} c_{k\alpha\sigma} + \sum_{k\alpha\sigma} \left(v c^{\dagger}_{k\alpha\sigma} d_{\alpha\sigma} + \text{H.c.} \right) + \sum_{\alpha\sigma} \epsilon^{2I} d^{\dagger}_{\alpha\sigma} d_{\alpha\sigma} + \sum_{\alpha} U^{2I} n_{\alpha\uparrow} n_{\alpha\downarrow} + J_z s^z_1 s^z_2 + \frac{J_\perp}{2} \left(s^+_1 s^-_2 + s^-_1 s^+_2 \right). \tag{8}$$

For simplicity we consider two equivalent channels, and $\alpha = 1, 2$ refers to both impurities.

Changing the basis of the four impurity states from the individual spin projections $|s^z_1 s^z_2\rangle$ to the total spin and projection $|SM\rangle$ with $S = 0, 1$, $M = -1, 0, 1$, and denoting by E_{SM} the energies of these states in the new basis, one obtains an effective Hund coupling $J_H = E_{00} - E_{10} = -J_\perp$ and an exchange anisotropy directly related with the single-ion anisotropy of the spin-1 model through the relation $D = E_{10} - E_{10} = \frac{1}{2}(J_z - J_\perp)$.

It is interesting to note that the properties of the system are invariant under a rotation of one of the impurity spins (for example s_2) in π around the z axis (or equivalently a change of sign of the states with $s^z_2 = -1/2$). This transformation changes the sign of $J_\perp$ and interchanges the states $|00\rangle$ and $|10\rangle$. In particular, the isotropic two-impurity model with $J_\perp = J_z > 0$ is mapped into our A2CS1KM model with $J_H = D = J_z$, for which one expects a topological phase for low or moderate T_K.

Therefore, the two-impurity system will undergo a TQPT depending on the exchange anisotropy. In fact, one of the first systems in which the existence of a non-trivial Fermi liquid was detected was the

two-impurity system in [15]. This significantly broadens the range of impurity systems in which the TQPT theory could be useful to interpret scanning-tunneling spectroscopy measurements.

Other equivalent models can be constructed interchanging the spin degree of freedom with the pseudospin one that takes into account the charge degrees of freedom. In fact, this equivalence has been used in section III B of [41] to map an Anderson model similar to ours to the corresponding version with pseudospin interactions. However, these models do not seem to be realistic.

5. Extension to larger spin

For impurities involving transition metal ions, the localized spin S can vary in the interval $0 \leqslant S \leqslant 5/2$. Clearly, for $S = 0$ there is no Kondo effect. The number of channels can also vary reaching up to 5 channels. Since treating more than two channels is computationally too expensive with the NRG, we restrict the present study to two channels, assuming for the moment equivalent channels.

The effects of anisotropy when only one channel is present was studied before [31–34]. For $S = 1$, the transition occurs at $D_c = 0^+$ [33, 34] and the Luttinger integral takes the value $\pi/2$ at this point [19]. For any single-channel $S \geqslant 1$ impurity, there is a competition between the underscreened Kondo effect [7] and the single-ion anisotropy for $D > 0$, giving rise to a complex low energy behavior that strongly depends on the integer or half-integer nature of S and the $D = 0$ Kondo temperature T_K (see table 1).

For two channels and $S = 1/2$, the anisotropy is irrelevant and one has a non-Fermi liquid behavior corresponding to the spin-1/2 2CKM [42]. The $S = 3/2$ case has been studied before with NRG [24, 25], and it was found that the two-channel Kondo effect also describes its low-energy physics as in the $S = 1/2$ case. On the other hand, for $S = 2$ we find a similar topological transition as for $S = 1$. Therefore, the low-temperature behavior can be divided into two groups depending if the spin is integer or a half-integer. Table 1 presents a summary of the different cases.

In figure 5 we show the evolution of the entropy with temperature for different spins and anisotropy. For $D = 0$ (orange curves), the two equivalent hybridizing channels reduce the ground state spin to a residual value $S' = S - 1$ and the entropy at zero temperature approaches $\ln(2S' - 1)$. For negative D (blue curves) the ground state is two-fold degenerate. The most interesting case is for positive D. In this case, for half-integer S the low-energy behavior is dominated by the physics of the spin-1/2 2CKM and the zero-temperature entropy is $\frac{1}{2}\ln(2)$. For integer S, the ground state is non-degenerate.

In figure 6 we show the conductance $G(T)$ (related to the spectral density) as a function of temperature for different S and D. For $D = 0$ (orange curves), $G(T)$ for $T \to 0$ tends to the unitary value $G_0 = 4e^2/h$, characteristic of two orbital- and spin-degenerate conduction channels. The case $D < 0$ is complex and is not of interest to the central objective of this article, because in such a case, there is no quantum phase transition. For $D > 0$ and half-integer S, the low-temperature value is $G_0/2$, characteristic of the spin-1/2 2CKM. For integer S, $G(0) = G_0$ (zero) if D is below (above) the critical anisotropy D_c of the topological transition. In the figure only the case $D > D_c$ is shown.

We have also analyzed what happens for the half-integer case when the couplings of the two channels are different in presence of a small $D > 0$. The ground state becomes a singlet and therefore, the entropy goes to zero for $T \to 0$. The contribution to the conductance of the channel with a larger coupling constant is similar to that of the simplest spin-1/2 1-channel Kondo model, increasing at T_K and reaching $2e^2/h$ at zero temperature. At a lower characteristic temperature the conductance of the other channel decreases with decreasing temperature, indicating a dip in the corresponding spectral density. This seems to be the case of MnPc on Au(111). See section 6.2.

6. Experimental relevance of the TQPT

In this section, we present several systems of atoms or molecules on metallic surfaces, and we show that scanning-tunneling spectroscopy experiments performed on them can be explained qualitatively or semiquantitatively by means of the two-channel $S = 1$ Kondo or Anderson models with anisotropy. In most of these cases, alternative explanations were proposed in the literature that contradict basic physical principles or are unsatisfactory. As the theory of the TQPT is relatively new and it seems to be only captured by NRG calculations, while alternative explanations fail, it is important to show that a consistent explanation using new concepts and models exists. This is our focus, and not to provide an accurate fit of all the experimental curves mentioned below, an objective that lies beyond the scope of this paper.

6.1. FePc on Au(111)

The system of iron phthalocyanine (FePc) on the Au(111) surface has attracted a lot of attention during the last 15 years [11, 39, 43–52]. According to LDA + U calculations, the basic electronic structure of the

Table 1. Low energy states for a magnetic impurity of spin S with $D > 0$ and coupled to $\#ch.$ equivalent conduction channels. KE = Kondo effect; FL = Fermi liquid. T_K is the Kondo temperature for $D = 0$.

# ch.	S	D	Low energy electronic state
1	1/2	Irrelevant	Fully compensated KE, conventional FL
1	Integer	$D_c = 0^+$	Two-stage KE: Effective (anisotropic) S = 1/2 KE for $D < T_K$; Quenched impurity spin for $D > T_K$ [31]
1	Half-integer	$D_c = 0^+$	Two-stage KE: quenched impurity spin for $D < T_K$; Effective and complex S = 1/2 KE for $D > T_K$ [31]
2	1/2	Irrelevant	Two-channel KE: non-Fermi liquid [7]
2	1	$D_c > 0$	$D < D_c$: fully compensated KE $D > D_c$: quenched impurity spin, *non-Landau* FL [8]
2	3/2	$D_c = 0^+$	Effective two-channel (anisotropic) KE [24]
2	2	$D_c > 0$	$D < D_c$: fully compensated KE $D > D_c$: quenched impurity spin, *non-Landau* FL [8]

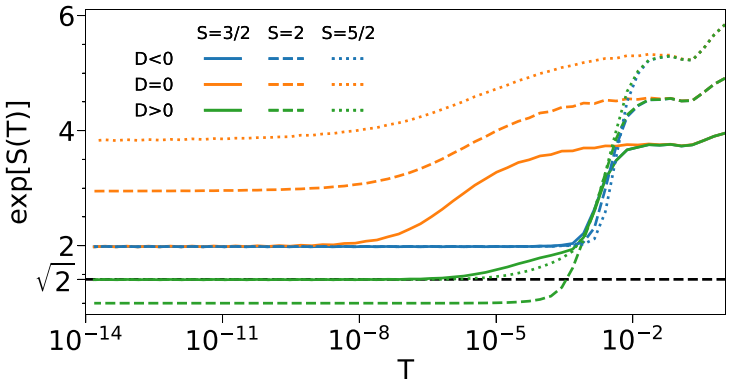

Figure 5. Entropy as a function of temperature for $J_K = 0.16$ and different values of S and D. $D > 0$ ($D < 0$) corresponds to $D = 0.002$ (-0.002). W is taken as the unit of energy.

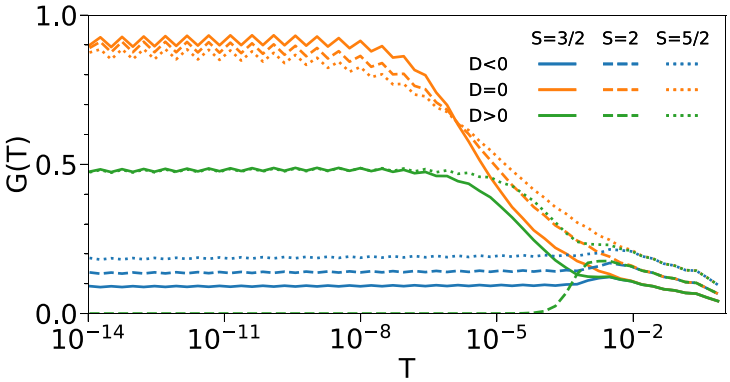

Figure 6. Conductance as a function of temperature for $J_K = 0.16$ and different S and D. $D > 0$ ($D < 0$) corresponds to $D = 0.002$ (-0.002). W is taken as the unit of energy.

molecule is that shown in figure 7, taken from [51]. The partially filled orbitals of Fe are those of symmetry $3z^2 - r^2$ with nearly one electron, and the degenerate so-called π orbitals, of symmetry xz and yz with three electrons, resulting in a spin 1. This is in agreement with x-ray magnetic circular dichroism experiments [44].

The differential conductance dI/dV observed by scanning-tunneling spectroscopy of a single FePc molecule on Au(111) in the on-top position shows a narrow dip mounted on a broad peak [46, 49, 52] (corresponding to the curves at the bottom of figures 8 and 9). This is very suggestive of the spectral density of localized electrons near the topological transition, for anisotropy D slightly larger than the critical one [8, 9] (see figure 1). However, most experiments were done before the development of the theory of the TQPT and were interpreted in a different fashion, as a two-stage Kondo effect: the $3z^2 - r^2$ orbitals hybridize strongly with the conduction electrons with the same symmetry, giving rise to a first-stage Kondo effect and

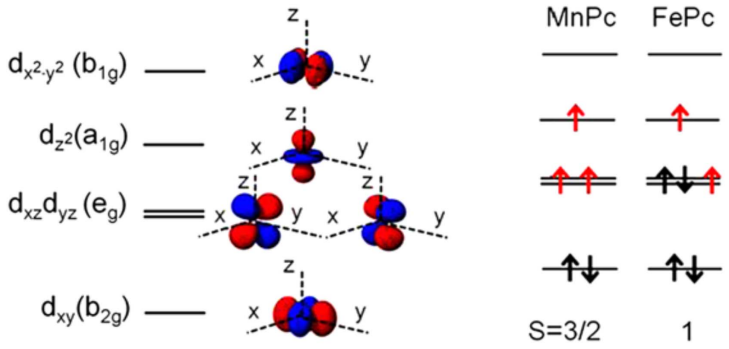

Figure 7. Electronic structure of MnPc and FePc. Reprinted with permission from [51]. Copyright (2020) American Chemical Society. Red arrows correspond to unpaired spins 1/2.

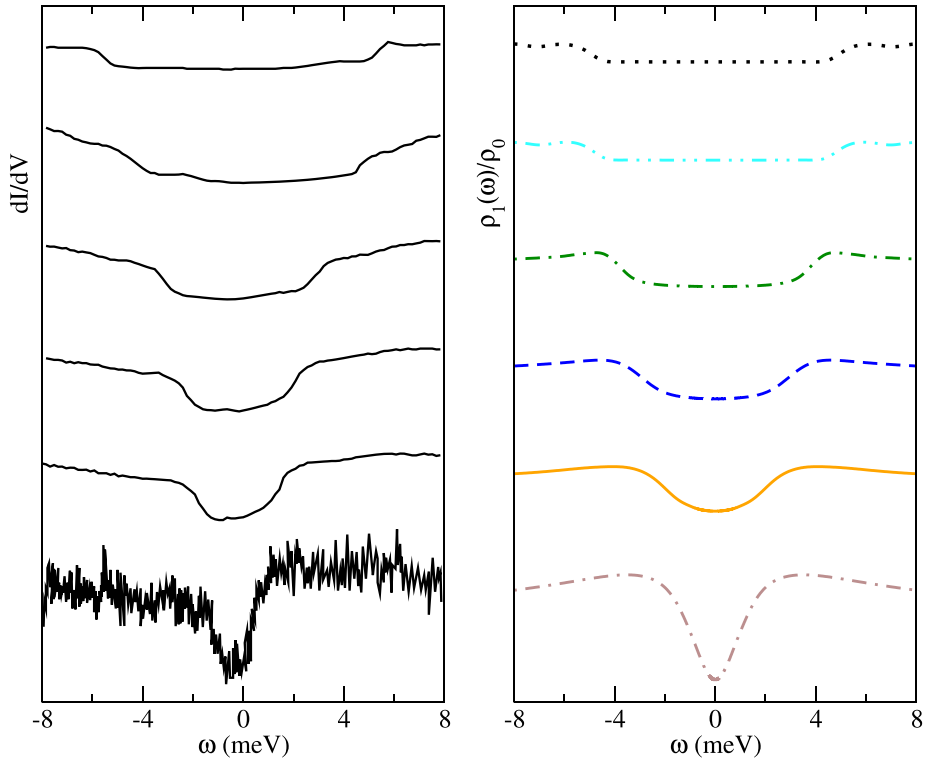

Figure 8. Left: experimental differential conductance of FePc on Au(111) as a function of voltage and right: theoretical spectral density of 3d $3z^2 - r^2$ electrons as a function of energy, as the molecule is raised from the surface. Parameters are $D = 0.005$ $J_z = 0.44f$, $J_a = 0.22f$ in units of the band width taken as 1 eV. From top to bottom, the factor f used is 0.1, 0.2, 0.5, 0.6, 0.7 and 0.8. (Left) Adapted from [49]. CC BY 4.0. (Right) Adapted from [11]. CC BY 4.0.

to the broad peak in $\mathrm{d}I/\mathrm{d}V$ around 20 meV. At a lower temperature, the Kondo effect due to the π orbitals sets in giving rise to a dip of half-width $\sim$0.6 meV in $\mathrm{d}I/\mathrm{d}V$ [46, 50]. The fits of the spectrum suggest the following hierarchy of the different orbitals in decreasing order of hopping amplitude to the tip: $3\mathrm{d}_{3z^2-r^2}$, conduction electrons with $3z^2 - r^2$ symmetry, conduction electrons with π symmetry and $3\mathrm{d}_{\pi}$ [50].

However, an experiment that can discern between both scenarios (TQPT or two-stage Kondo effect) has been made. Raising the FePc molecule from the surface [49], the hybridization amplitudes are weakened and, with them, the exchange interactions between localized 3d electrons and conduction electrons. In the two-stage scenario explained above one expects that both features, the broad peak and the Kondo dip *narrow* since the corresponding Kondo temperatures should decrease. Instead, if the system is a *non-Landau* Fermi liquid close to the topological transition, decreasing the exchange interactions with respect to D should *broaden* the dip as the system moves away from the TQPT. This last scenario is what is observed experimentally (see figure 8), giving support to the TQPT picture.

To construct the adequate model for FePc, one has to take into account the splitting of the π orbitals as a consequence of the SOC [39], neglected in previous treatments. The states $|\pi\sigma\rangle$ with one hole in the π

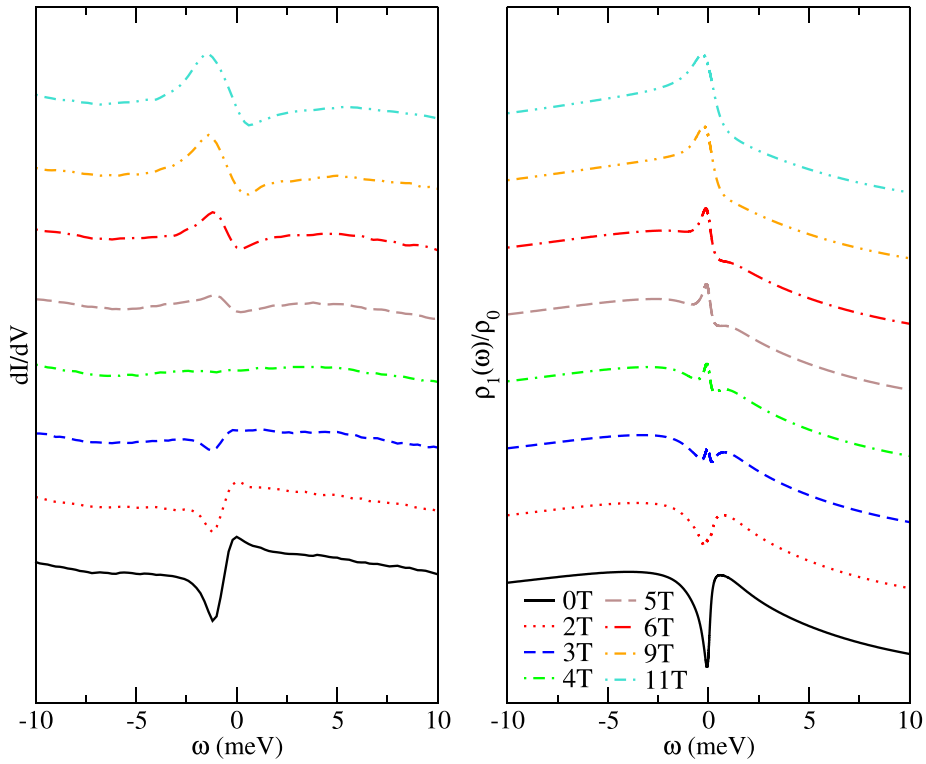

Figure 9. Experimental (left) and theoretical (right) differential conductance of FePc on Au(111) as a function of voltage for several values of the magnetic field. The experimental curves are adapted from [52]. CC BY 4.0, while the theoretical curves are reproduced from [11]. CC BY 4.0. Parameters as in figure 8 with $f = 1$ and asymmetry parameter $q = 0.4$.

orbitals are (except for an irrelevant phase)

$$|a\uparrow\rangle = \frac{|xz\uparrow\rangle + i|yz\uparrow\rangle}{\sqrt{2}}, |a\downarrow\rangle = \frac{|xz\downarrow\rangle - i|yz\downarrow\rangle}{\sqrt{2}},$$
$$|b\uparrow\rangle = \frac{|xz\uparrow\rangle - i|yz\uparrow\rangle}{\sqrt{2}}, |b\downarrow\rangle = \frac{|xz\downarrow\rangle + i|yz\downarrow\rangle}{\sqrt{2}}. \quad (9)$$

The $|b\sigma\rangle$ states lie above the $|a\sigma\rangle$ by an energy of the order of the SOC, estimated in 76 meV for Fe [53]. This also leads to a significant orbital polarization which was observed [44], and to an anisotropy $D \sim 5$ meV.

Therefore, an appropriate model to describe the system is the A2CS1KM, one channel with strong exchange coupling J_z for the $3z^2 - r^2$ electrons and another channel of the a states J_a. The effect of raising the molecule is incorporated in our model by reducing both J_z and J_a by the same factor f. In this way, the experiments can be semiquantitatively explained [11], as shown in figure 8.

In [52] the dependence of $G = \mathrm{d}I/\mathrm{d}V$ with temperature and magnetic field has been measured. The results have been also explained using the A2CS1KM [11]. As the temperature is raised, the dip is reduced and disappears at ~ 10 K. The dependence with the magnetic field shown in figure 9 is striking: the narrow dip is converted into a narrow peak as the magnetic field is increased. The theoretical results, taken from [11], reproduce semiquantitatively the experimental data. To take into account the asymmetry of the shape, we assume that the STM tip senses mainly the localized electrons of symmetry $\tau = 3z^2 - r^2$ with some admixture of conduction electrons with the same symmetry weighted by the parameter q [54], which we take as $q = 0.4$. The conductance given by our model G_m, represented at the right of figure 9 is therefore given by [11]:

$$G_m(V) = -\left[\left(1 - q^2\right) \mathrm{Im}G^d_{\tau\sigma}(\omega) + 2q\mathrm{Re}G^d_{\tau\sigma}(\omega)\right], \quad (10)$$

where $G^d_{\tau\sigma}(\omega)$ is the Green function of localized electrons for symmetry τ and spin σ.

A better agreement can probably be obtained by enlarging J_z, which has the effect of broadening the broad peak, adjusting J_a to broaden the dip a little bit, and by including the orbital polarization, which increases the effective coupling with the magnetic field by a factor of 3/2.

6.2. MnPc on Au(111)

Curiously, in spite of having one electron less than FePc, the observed differential conductance in Mn phthalocyanine on Au(111) [55] is qualitatively very similar to that observed in the Fe system. There is a dip

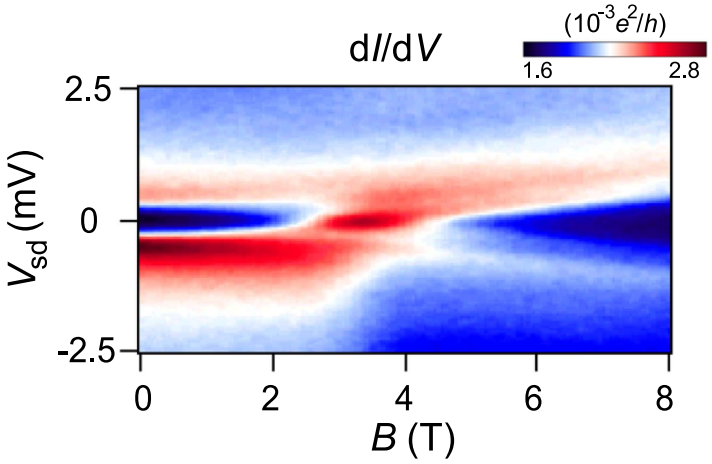

Figure 10. Differential conductance $\mathrm{d}I/\mathrm{d}V$ of MnPc on Au(111) as a function of magnetic field B and bias voltage V_{sd}. Reproduced from [55]. CC BY 4.0.

of half-width about 0.5 mV, mounted on a broad peak. Under the application of a magnetic field, the dip turns to a peak at ~ 4 Tesla, and for a larger magnetic field the peak splits (see figure 10). The latter behavior was not observed in the FePc system, but is expected if larger fields were applied in that case.

It has been suggested that the observed behavior can be explained by a singlet ground state and a triplet excited state with a small excitation energy [55]. However, on one hand, the Hund coupling in 3d transition-metal elements are of the order of 0.7 eV, favoring a total spin 3/2. On the other hand, specific calculations for the singlet-triplet model with a small triplet excitation energy shows a $\mathrm{d}I/\mathrm{d}V$ that *decreases* slightly with increasing temperature T for small T (see figure 7 of [20]), in contrast to the experimental observations [figure 2(b) of [55]].

The calculated electronic structure for planar MnPc, is different from that in the gas phase (represented in figure 7) and corresponds to the intermediate-spin quartet ${}^4E_g$ $[(xy)^1(\pi)^3(3z^2-r^2)^1]$ [56, 57]. This is in agreement with polarization-dependent N K-edge x-ray absorption spectra for MnPc on Au [58]. Therefore, the difference with the electronic structure for FePc on Au(111) is that, in the Mn system, there is a hole in the $3d_{xy}$ which is absent in the Fe system, leading to total spin 3/2 in the Mn case.

A realistic model for MnPc on Au(111) involves therefore three channels [states with symmetry $3z^2-r^2$, a of equation (9) and xy] and is almost intractable with NRG. In order to have a qualitative understanding, we have studied a spin 3/2, 2CKM including anisotropy, assuming $J_z \sim 2J_a$ and $J_{xy}=0$. From the temperature dependence of the conductance, we see a first-stage Kondo effect in which the contribution of the dominant $3z^2-r^2$ channel is the usual one for a spin 1/2 system, saturating near $2e^2/h$ at low temperatures, without a dip. However, the contribution of the a channel has a dip, so that the total conductance presents a narrow dip mounted on a broad peak. The ground state is a singlet.

The results can be qualitatively understood as follows. At temperatures of the order of the Kondo temperature of the dominant $3z^2-r^2$ channel (near 20 meV in the Fe system), the spin of that channel is screened and one is left with a spin 1 screened partially by the exchange in the a channel and with anisotropy D. This model has been studied and, in presence of any $D>0$ [33, 34], the conductance and the spectral density have a dip, whose width decreases exponentially with $\sqrt{D}$, while the application of a magnetic field leads to a differential conductance of the same form as that shown in figure 10 of [34]. If, in the effective model after screening the spin 1/2 of the dominant channel, one includes the exchange of the third channel xy, the model is precisely the A2CS1KM, and one expects a TQPT at finite D. The parameters should be renormalized, as expected from approximate treatments of similar 3-channel models [50].

Other impurity systems containing phthalocyanine molecules, such as CoPc on Au(111) [59] and TiPc on Cu(110) [60] were also studied, where the low-energy physics seems dominated by the usual Kondo effect.

6.3. Nickelocene on Cu(100)

The system of isolated double-decker nickelocene (Nc) molecules on Cu(100) substrates have been experimentally studied in detail [27, 61–66]. Density functional theory (DFT) calculations show that the electronic structure of Ni is basically $3d^8$, with one hole in each of the nearly degenerate π orbitals (xz and yz), with some mixing with the $3d^9$ configuration [27, 63]. Therefore the appropriate model to describe the system is actually the 2CS1AMA proposed for Ni impurities in a Au chain doped with oxygen [8, 9] or its integer-valent limit, the A2CS1KM [9].

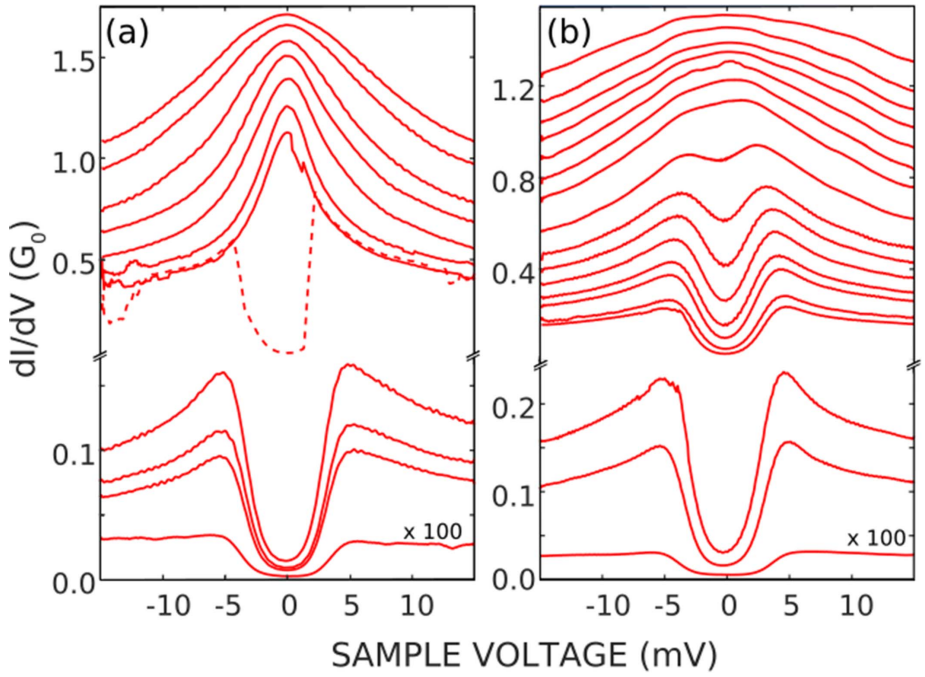

Figure 11. Differential conductance of several samples of Nc on Cu(111) (a) [(b)] correspond to spectra observed with frequency 2/3 [1/3], approximately. Within each panel, the higher a curve is, the shorter the distance from the molecule to the substrate. Reprinted (figure) with permission from [27], Copyright (2020) by the American Physical Society.

The experimentally observed spectra for the differential conductance $\mathrm{d}I/\mathrm{d}V$ are shown in figure 11. Left and right panels correspond to spectra observed with frequency 2/3 (case A) and 1/3 (cases B), respectively. The curves within each panel correspond to different positions of the tip. As the STM tip is approached to the molecule, the hybridization between tip and molecule states increases and a jump from a dip to a peak near $V = 0$ takes place, which is consistent with the TQPT.

In the theory that was presented alongside the experimental observations, the occurrence of a peak or a dip has been tentatively ascribed to a crossover in the spin of the molecule. This transition is noted as shifting from 1/2 in the contact regime (STM tip near the molecule) to 1 in the tunneling regime (STM tip far from the molecule), a deduction based on first-principle calculations [27, 63]. However, on one hand, these calculations miss relevant dynamical correlations and, therefore, they do not properly treat the Kondo effect which tends to screen the spin. On the other hand, the electronic structure does not change much between the two regimes and, as admitted by the authors, the change in the molecular charge is actually insufficient to account for the large change in the spin.

The observed spectra have many similarities with the spectral density of localized electrons in the A2CS1KM (see figure 1) but also important differences. For case A, there seems to be a first-order transition as the tip is approached to the molecule, avoiding the transition zone with a very narrow peak or dip, as shown in figure 1. For case B, the transition seems to be continuous, without a jump from a dip to a peak at zero voltage, as the hybridization (or exchange) between localized and conduction electrons is increased.

The first-order transition of case A can be understood as follows: as in FePc on Au(111), in which the molecule is raised when the STM approaches it [49], we expect that some variable η which determines either the position or the shape of the molecule, modifies the hybridization v of the 2CS1AMA [equation (2) assuming $v_\tau = v$, the same for both channels] [28], leading to a coupling of η with our electronic model. In the absence of this coupling, one expects that the elastic energy is $E_\mathrm{e} = K\eta^2/2$ (shifting the 0 of η if necessary). It has been shown that the second derivative of the energy of the electronic model is strong and negative near the TQPT [28]. This means that for a soft spring (small K) the second derivative of the total energy is also negative at the TQPT, leading to a first-order transition in a Maxwell construction [28]. This reasoning provides a natural explanation of the observed behavior for case A.

Case B probably corresponds to a hard spring (large K) and the first-order transition does not take place. The reason why an abrupt jump like that in figure 1 is not observed is two-fold: i) the magnitude of the jump decreases with the degree of intermediate valence [see equations (3) and (4)] and ii) finite temperature. This is the most relevant parameter. These effects were investigated using the 2CS1AMA described by equation (2) [28]. In figure 12 we show the evolution of the differential conductance for different values of

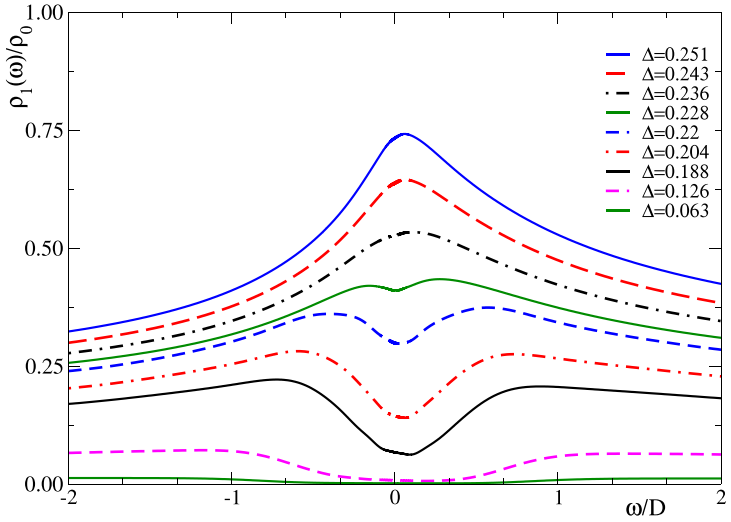

Figure 12. Differential conductance as a function of voltage for different values of Δ. Other parameters are $U = 3.5$, $U' = 2.5$, $J_H = 0.5$, $\epsilon = -3.0$, $T = 0.0005$ [see equation (2)].

$\Delta = \pi v^2 \rho_c$ where $\rho_c = 1/(2W)$ is the density of conduction electrons assumed constant in the range $-W < \omega < W$. The half-band width $W = 1$ eV is taken as the unit of energy. For small Δ, dI/dV has a dip mounted on a broader peak, as usual. As Δ increases, the dip narrows, but in contrast to the case of zero temperature, the minimum of the dip increases, and a very sharp dip like that of figure 1 is absent. For larger Δ the dip gradually disappears and the magnitude of dI/dV near zero voltage increases. The overall behavior reproduces semiquantitatively the experimental results for case B shown in the right panel of figure 11.

6.4. Fe Atoms on MoS_2/Au(111)

Trishin *et al* [67] studied experimentally a system consisting of an Fe atom on top of a monolayer of MoS_2 deposited in turn on a Au(111) surface. As argued below, it is very natural to expect that the system is described by the A2CS1KM. MoS_2 on Au(111) forms a Moiré structure, which implies strong local variations of the density of conduction electrons ρ_c. Therefore, depending on the specific position at which the Fe adatom is located, dramatic variations of the adimensional parameter $J' = \rho_c J_K$ (which determines the Kondo temperature) are expected, and one might expect to observe the TQPT as in figure 1.

The validity of the A2CS1KM to describe the system can be justified as follows. DFT calculations of Fe atoms on free-standing MoS_2 indicates that the spin state of the atoms is either $S = 1$ [68] or $S = 2$ [69]. However, for $S = 2$, one would expect a second jump in $G(V)$ at larger $|V|$ in the regime of low J', which is not observed experimentally [figure 3(h) of [67]]. On the other hand, experiments and DFT calculations indicate that the Fe atoms are located in positions with symmetry corresponding to the point group C_{3v}. Therefore, the Fe $3d$ orbitals are split into one A_1 singlet and two E doublets [70]. Our comparison with the experiment (shown in figure 13), indicates that the spin 1 is formed by occupying the two states of an E doublet (the agreement worsens when non-equivalent channels are considered). In this case, it is clear that the SOC originates a hard axis anisotropy $D(S_z)^2$ with $D > 0$ [28]. In addition, each of the degenerate orbitals of the doublet hybridizes with conduction states of the same symmetry [8, 9, 28]. This reasoning naturally leads to the 2CS1AMA with degenerate channels used in references [8, 9, 28] and to the A2CS1KM in the integer valence limit.

The differential conductance $G(V) = dI/dV$ has been measured on nearly 40 different Fe positions. Six of them [(a) to (f)] are presented in [67] and five of them [(b) to (f)] are reproduced in our figure 13. In [67], fits of the different spectra were done using three different approaches: i) perturbation theory in the exchange coupling in an $S = 1$ anisotropic one-channel Kondo model for cases (a) to (d), ii) a Frota peak (expected for the simplest Kondo model) for case (f), and iii) a Lorentz peak plus Frota dip (without justification) for case (e). Note that the fit of the peak and the dip requires 3 parameters for each one (determining position, width and intensity) in addition to a linear background. Therefore the resulting good fit is not surprising [67], but it lacks a physical justification.

In contrast, as shown in Fig 13, the A2CS1KM can semiquantitatively explain the data in a unified fashion. A better agreement with the experiment can be obtained by allowing some degree of intermediate valence for cases (e) and (f), as explained below, but we wanted to keep the number of free parameters as minimal as possible.

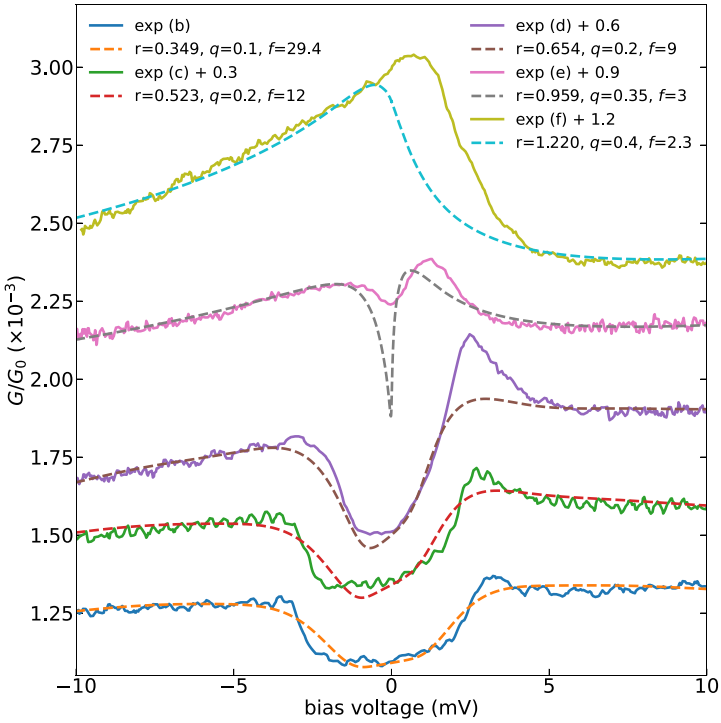

Figure 13. Differential conductance corresponding to the experimental curves (b) to (f) (full lines, each curve is labeled as exp(b),etc) and the results for our model (dashed lines,shifted upward by the same magnitude as the corresponding experimental curve). Note that (a) is not included and the top figure corresponds to (b). See the main text for the meaning of the r, q and f fitting parameters. Adapted (figure) with permission from [28], Copyright (2023) by the American Physical Society.

The numerical calculations were performed with the Ljubljana code of the NRG [29, 30], and were reported previously in [71]. We assume flat conduction bands extending from $-W$ to W for both symmetries. We take $W = 1$ eV and $D = 2.7$ meV. The product $J' = \rho_c J_K$ is assumed to vary among the different cases, due to the Moiré modulation. The TQPT is at $J'_c \sim 0.135$. The different theoretical curves in figure 13 correspond to different values of the ratio $r = J'/J'_c$.

The structure at low voltage V of the differential conductance $G(V) = \mathrm{d}I/\mathrm{d}V$ is determined by the localized and conduction electrons of symmetry τ included in the model. We assume that the STM tip senses mainly the localized $3d$ states with some admixture of conduction states. Thus, the contribution of the model to $G(V)$ at zero temperature is given by equation (10), where the Green functions $G^d_{\tau\sigma}(\omega)$ depend only on r, and q is a measure of the contribution of the conduction states. In the experiment, there is also a linear background due to the contribution of other states, and $G_m(V)$ is affected by a factor f which depends on the distance of the STM tip to the system. Therefore, to fit the experiment, the following expression is used

$$G(V) = fG_m(V) + A + BV, \tag{11}$$

which contains five parameters (r, f, q, A and B), but the *shape* of each curve depends essentially on r, while q controls the asymmetry. We have not included in the comparison with experiments the curve (a), which is similar to a rectangular dip formed by two step-like functions, because these steps are overbroadened in our calculations due to the limited resolution of the NRG at large energies [35].

The agreement between theory and experiment for cases (e) and (f) could be considerably improved by introducing intermediate valence effects. This is in fact expected since a larger conduction density of states increases the parameter $\Delta = \pi \nu^2 \rho_c$ discussed in section 6.3, which controls the degree of intermediate valence. It is well known that a smaller occupancy of the localized states shifts the Kondo peak to higher energies. Concerning case (e), the dip in the theory is more pronounced than in the experiment. However, as shown in section 6.3, intermediate valence and finite temperature reduces the magnitude of the dip compared to that predicted by the A2CS1KM.

The comparison with the experiment can also be affected by the assumption of a constant density of conduction states and the effect of other orbitals not considered in our model. In any case, the experimental and theoretical results, including the LDA and NRG ones, strongly suggests that the underlying physics is that of the 2CS1AMA.

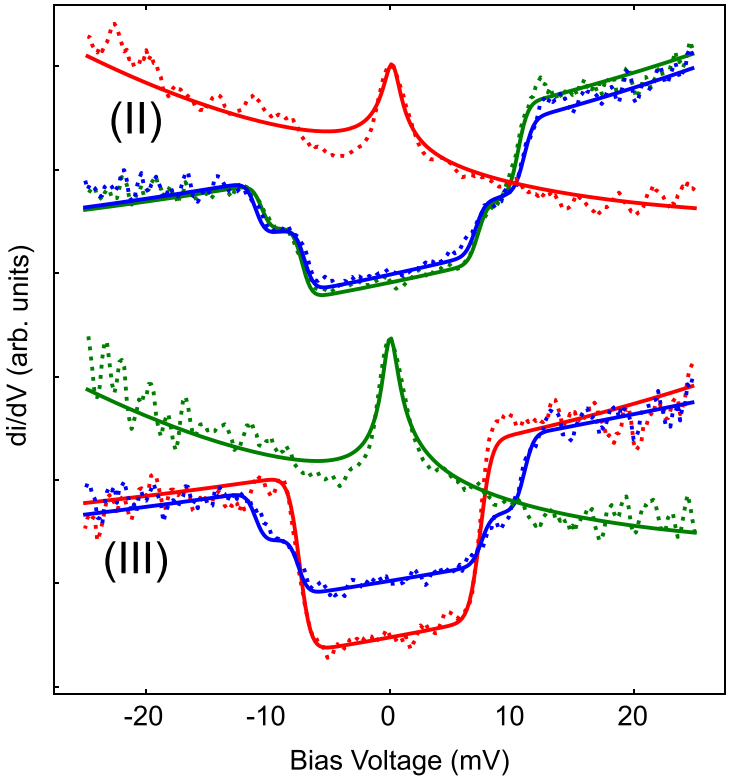

Figure 14. Differential conductance obtained at different positions (II and III) of a chain of three Fe-porphyrin-based molecules on top of herringbone-reconstructed Au(111) containing a Br atom. The presence of a peak (dip) signals a molecule in a 'Kondo' ('spin-flip') position. The solid curves correspond to phenomenological fits of the data. Reprinted with permission from [73]. Copyright (2023) American Chemical Society.

6.5. Fe porphyrin molecules on Au(111)

Experiments similar to those for the Nc molecule on Cu(100) (see section 6.3), in which the STM tip is approached to the molecule, have been carried out for iron porphyrin molecules on Au(111) [72]. The LDA calculations indicate that the Fe spin is 1, with a partial occupancy of two orbitals (of symmetry $3z^2 - r^2$ and $x^2 - y^2$), that belong to different irreducible representations. In other words, the two channels are not equivalent. One expects that the A2CS1KM or the corresponding Anderson model with non-equivalent channels, should be appropriate for the system. In these experiments, the dip narrows as the contact regime is approached, but never turns to a peak, in contrast to Nc on Cu(100). Nevertheless, the results are consistent with our model assuming a weaker hybridization of the localized states with the substrate in comparison to Nc/Cu(100).

More recently similar experiments have been carried out using a Br decorated Au(111) surface [73]. In this case, depending on the particular position of the molecule with respect to the defects, sometimes a broad dip is observed and sometimes a narrow peak (see figure 14), consistent with the A2CS1KM for parameters near the TQPT on the non-trivial and trivial topological sectors, respectively.

7. Summary and discussion

Since the seminal work of Nozières and Blandin [7], the Kondo effect in situations involving multiorbital magnetic impurities and/or coupled to more than one conduction channels has become a highly active area of research within condensed matter physics. The primary motivation stems from the prediction of exotic electronic states, such as non-Fermi liquids (overscreened Kondo effect) and singular Fermi liquids (underscreened Kondo effect), exhibiting distinctive dynamic and thermal behaviors, that, on one hand, could shed light on unconventional physics in heavy fermion compounds, and, on the other hand, they serve as paradigmatic models for quantum many-body phenomena.

The simplest generalization of the conventional Kondo effect to multiorbital systems, where a spin $S > 1/2$ is fully screened by $n = 2S$ channels, has been relatively underexplored, perhaps because it was believed that no new physics could be found in this context. However, we have shown in a series of recent publications that the presence of single-ion magnetic anisotropy drives these systems through a TQPT, that separates two topologically distinctive local Fermi liquids.

Besides the theoretical relevance of our finding, we have shown that several systems consisting of isolated magnetic atoms or molecules on noble metal surfaces can be described by the 2CS1AMA or its integer valent limit, the A2CS1KM. Both models exhibits the TQPT, as a consequence of which the spectral density at zero temperature of the localized electrons has a jump between high values in the topologically trivial Fermi liquid phase to very low values in the non-trivial "non-Landau" Fermi liquid phase. Near the transition, the spectral density is characterized by a narrow peak or dip (depending on the phase) mounted on a broad peak.

It is worth clarifying that the topological transition studied in this work has a local character, as it pertains solely to the impurity's degrees of freedom. Furthermore, the topological properties arise from the frequency dependence of the impurity's Green's function, rather than from the momentum dependence, as is typically the case in the far more studied topological systems in condensed matter physics.

The abrupt transition might have technological applications. For example the system can act as a transistor, which is one of the most important components of an integrated circuit, as it acts as a switch by changing some parameter [4]. It also enlarges the field of single-molecule switches [74] and bistable molecular systems [75].

Several experiments with scanning-tunneling spectroscopy in different systems have in fact identified similar structures in the differential conductance. Five of these systems are listed in section 6. They were usually interpreted using different, more conventional theories, probably due to the fact of the novelty of the concepts related to the TQPT. We expect that this work contributes to disseminate these rather novel ideas to the community of condensed-matter and nanoscience researchers.

We have also shown that the concepts can be extended to larger spin and two-impurity systems.

Data availability statement

All data that support the findings of this study are included within the article (and any supplementary files).

Acknowledgments

We thank Rok Žitko and Pablo Roura-Bas for several collaborations in subjects of this review. AAA acknowledges financial support provided by PICT 2018-01546 and PICT 2020A-03661 of the Agencia I+D+i, Argentina. LOM and GGB acknowledge financial support provided by PIP 3220 of CONICET, Argentina.

ORCID iDs

G G Blesio https://orcid.org/0000-0002-1962-0969
L O Manuel https://orcid.org/0000-0001-7793-1709
A A Aligia https://orcid.org/0000-0001-9647-3926

References

[1] Yang K, Paul W, Phark S H, Willke P, Bae Y, Choi T, Esat T, Ardavan A, Heinrich A J and Lutz C P 2019 Coherent spin manipulation of individual atoms on a surface *Science* **366** 509
[2] Aradhya S V and Venkataraman L 2013 Single-molecule junctions beyond electronic transport *Nat. Nanotechnol.* **8** 399
[3] Cuevas J C and Scheer E 2010 *Molecular Electronics: An Introduction to Theory and Experiment* (World Scientific)
[4] Mathew P T and Fang F 2018 Advances in molecular electronics: a brief review *Engineering* **4** 760
[5] Kügel J, Karolak M, Krönlein A, Serrate D, Bode M and Sangiovanni G 2018 Reversible magnetic switching of high-spin molecules on a giant Rashba surface *npj Quantum Mater.* **3** 53
[6] Evers F, Korytár R, Tewari S and van Ruitenbeek J 2020 Advances and challenges in single-molecule electron transport *Rev. Mod. Phys.* **92** 035001
[7] Nozieres P and Blandin A 1980 Kondo effect in real metals *J. Phys. France* **41** 193
[8] Blesio G G, Manuel L O, Roura-Bas P and Aligia A A 2018 Topological quantum phase transition between Fermi liquid phases in an Anderson impurity model *Phys. Rev.* B **98** 195435
[9] Blesio G G, Manuel L O, Roura-Bas P and Aligia A A 2019 Fully compensated Kondo effect for a two-channel spin $S = 1$ impurity *Phys. Rev.* B **100** 075434
[10] Luttinger J M and Ward J C 1960 Ground-state energy of a many-fermion system. II *Phys. Rev.* **118** 1417
[11] Žitko R, Blesio G G, Manuel L O and Aligia A A 2021 Iron phthalocyanine on Au(111) is a "non-Landau" Fermi liquid *Nat. Commun.* **12** 6027
[12] Pustilnik M, Borda L, Glazman L I and von Delft B 2004 Quantum phase transition in a two-channel-Kondo quantum dot device *Phys. Rev.* B **69** 115316
[13] Fritz L and Vojta M 2004 Phase transitions in the pseudogap Anderson and Kondo models: Critical dimensions, renormalization group and local-moment criticality *Phys. Rev.* B **70** 214427
[14] Vojta M 2006 Impurity quantum phase transitions *Phil. Mag.* **86** 1807
[15] Curtin O J, Nishikawa Y, Hewson A C and Crow D J G 2018 Fermi liquids and the Luttinger theorem *J. Phys. Commun.* **2** 031001

[16] Nishikawa Y, Curtin O J, Hewson A C and Crow D J G 2018 Magnetic field induced quantum criticality and the Luttinger sum rule *Phys. Rev.* B **98** 104419
[17] Mitchell A K, Logan D E and Krishnamurthy H R 2011 Two-channel Kondo physics in odd impurity chains *Phys. Rev.* B **84** 035119
[18] Allub R and Aligia A A 1995 Ground state and magnetic susceptibility of intermediate-valence Tm impurities *Phys. Rev.* B **52** 7987
[19] Logan D E, Wright C J and Galpin M R 2009 Correlated electron physics in two-level quantum dots: Phase transitions, transport and experiment *Phys. Rev.* B **80** 125177
[20] Roura Bas P and Aligia A A 2010 Nonequilibrium dynamics of a singlet-triplet Anderson impurity near the quantum phase transition *J. Phys.: Condens. Matter* **22** 025602
[21] Florens S, Freyn A, Roch N, Wernsdorfer W, Balestro F, Roura-Bas P and Aligia A A 2011 Universal transport signatures in two-electron molecular quantum dots: gate-tunable Hund's rule, underscreened Kondo effect and quantum phase transitions *J. Phys.: Condens. Matter* **23** 243202
[22] Logan D E, Tucker A P and Galpin M R 2014 Common non-Fermi liquid phases in quantum impurity physics *Phys. Rev.* B **90** 075150
[23] Mitchell A K, Jarrold T F, Galpin M R and Logan D E 2013 Local moment formation and Kondo screening in impurity trimers *J. Phys. Chem.* B **42** 12777
[24] Di Napoli S, Weichselbaum A, Roura-Bas P, Aligia A A, Mokrousov Y and Blügel S 2013 Non-Fermi-liquid behavior in transport through Co-Doped Au chains *Phys. Rev. Lett.* **110** 196402
[25] Di Napoli S, Roura-Bas P, Weichselbaum A and Aligia A A 2014 Non-Fermi-liquid behavior in nonequilibrium transport through Co-doped Au chains connected to fourfold symmetric leads *Phys. Rev.* B **90** 125149
[26] Di Napoli S, Barral M A, Roura-Bas P and Manuel L O 2015 Llois A M and Aligia A A 2015 Kondo physics in a Ni impurity embedded in O-doped Au chains *Phys. Rev.* B **92** 085120
[27] Mohr M, Gruber M, Weismann A, Jacob D, Abufager P, Lorente N and Berndt R 2020 Spin dependent transmission of nickelocene-Cu contacts probed with shot noise *Phys. Rev.* B **101** 075414
[28] Blesio G G, Žitko R, Manuel L O and Aligia A A 2023 Topological quantum phase transition of nickelocene on Cu(100) *SciPost Phys.* **14** 042
[29] Žitko R and Pruschke T 2009 Energy resolution and discretization artifacts in the numerical renormalization group *Phys. Rev.* B **79** 085106
[30] Žitko R 2022 NRG Ljubljana-open source NRG code (available at: https://github.com/rokzitko/nrgljubljana)
[31] Žitko R, Peters R and Pruschke T 2008 Properties of anisotropic magnetic impurities on surfaces *Phys. Rev.* B **78** 224404
[32] Žitko R and Pruschke T 2010 Many-particle effects in adsorbed magnetic atomswith easy-axis anisotropy: the case of Fe on the CuN/Cu(100) surface *New J. Phys.* **12** 063040
[33] Parks J J *et al* 2010 Mechanical control of spin states in spin-1 molecules and the underscreened Kondo effect *Science* **328** 1370
[34] Cornaglia P S, Roura-Bas P, Aligia A A and Balseiro C A 2011 Quantum transport through a stretched spin-1 molecule *Europhys. Lett* **93** 47005
[35] Bulla R, Costi T and Pruschke T 2008 The numerical renormalization group method for quantum impurity systems *Rev. Mod. Phys.* **80** 395
[36] Langreth D C 1966 Friedel sum rule for Anderson's model of localized impurity states *Phys. Rev.* **150** 516
[37] Yoshimori A and Zawadowski A 1982 Restricted Friedel sum rules and Korringa relations as consequences of conservation laws *J. Phys. C: Solid State Phys.* **15** 5241
[38] Seki K and Yunoki S 2017 Topological interpretation of the Luttinger theorem *Phys. Rev.* B **96** 085124
[39] Aligia A A 2022 Low-energy physics for an iron phthalocyanine molecule on Au(111) *Phys. Rev.* B **105** 205114
[40] Ternes M 2015 Spin excitations and correlations in scanning tunneling spectroscopy *New J. Phys.* **17** 063016
[41] De Leo L and Fabrizio M 2004 Spectral properties of a two-orbital Anderson impurity model across a non-Fermi-liquid fixed point *Phys. Rev.* B **69** 245114
[42] Mitchell A K, Sela E and Logan D E 2012 Two-channel Kondo physics in two-impurity Kondo models *Phys. Rev. Lett.* **108** 086405
[43] Gao L *et al* 2007 Site-Specific Kondo Effect at Ambient Temperatures in Iron-Based Molecules *Phys. Rev. Lett.* **99** 106402
[44] Bartolomé J, Bartolomé G L M, Filoti G, Gredig T, Colesniuc C N, Schuller I K and Cezar J C 2010 Highly unquenched orbital moment in textured Fe-phthalocyanine thin films *Phys. Rev.* B **81** 195405
[45] Tsukahara N, Shiraki S, Itou S, Ohta N, Takagi N and Kawai M 2011 Evolution of Kondo resonance from a single impurity molecule to the two-dimensional lattice *Phys. Rev. Lett.* **106** 187201
[46] Minamitani E, Tsukahara N, Matsunaka D, Kim Y, Takagi N and Kawai M 2012 Symmetry-driven Novel Kondo effect in a molecule *Phys. Rev. Lett.* **109** 086602
[47] Lobos A M, Romero M A and Aligia A A 2014 Spectral evolution of the SU(4) Kondo effect from the single impurity to the two-dimensional limit *Phys. Rev.* B **89** 121406(R)
[48] Fernández J, Aligia A A and Lobos A M 2015 Valence fluctuations in a lattice of magnetic molecules: application to iron(II) phthalocyanine molecules on Au(111) *Europhys. Lett* **109** 37011
[49] Hiraoka R, Minamitani E, Arafune R, Tsukahara N, Watanabe S, Kawai M and Takagi N 1027 Single-molecule quantum dot as a Kondo simulator *Nat. Commun.* **8** 16012
[50] Fernéndez J, Roura-Bas P, Camjayi A and Aligia A A 2018 Two-stage three-channel Kondo physics for an FePc molecule on the Au(111) surface *J. Phys.: Condens. Matter* **30** 374003
Fernéndez J, Roura-Bas P, Camjayi A and Aligia A A 2018 *J. Phys.: Condens. Matter* **31** 029501 corrigendum)
[51] Aykanat A, Meng Z, Benedetto G and Mirica K A 2020 Molecular engineering of multifunctional metallophthalocyanine containing framework materials *Chem. Mater.* **32** 5372
[52] Yang K *et al* 2019 Tunable giant magnetoresistance in a single-molecule junction *Nat. Commun.* **10** 1038
[53] Fisk C, Valdemoro C and Fraga S 1968 Spin-orbit coupling in some positive ions of Cr, Mn and Fe *J. Chem. Phys.* **48** 2923
[54] Žitko R 2011 Kondo resonance lineshape of magnetic adatoms on decoupling layers *Phys. Rev.* B **84** 195116
[55] Guo X, Zhu Q, Zhou L, Yu W, Lu W and Lian W 2021 Evolution and universality of two-stage Kondo effect in single manganese phthalocyanine molecule transistors *Nat. Commun.* **12** 1566
[56] Liao M-S, Watts J D and Huang M J 2005 DFT Study of Unligated and Ligated Manganese II Porphyrins and Phthalocyanines *Inorg. Chem.* **44** 1941
[57] Brumboiu I E *et al* 2014 Elucidating the 3d electronic configuration in manganese phthalocyanine *J. Phys. Chem.* A **118** 927
[58] Petraki F, Peisert H, Hoffmann P, Uihlein J, Knupfer M and Chasse T 2012 Modification of the 3d-electronic configuration of manganese phthalocyanine at the interface to gold *J. Phys. Chem.* C **116** 5121

[59] Wang Y, Zheng X, Li B and Yang J 2014 Understanding the Kondo resonance in the d-CoPc/Au(111) adsorption system *J. Phys. Chem.* **141** 084713
[60] Ribeiro L C , Lopes V, Chiappe G, Louis E and Anda E V 2024 Kondo effect in distorted titanium phthalocyanine molecules adsorbed on a Cu(110) metallic surface *J. Phys. Chem.* C **128** 8767
[61] Bachellier N, Ormaza M, Faraggi M, Verlhac B, Vérot M, Le Bahers T, Bocquet M-L and Limot L 2016 Unveiling nickelocene bonding to a noble metal surface *Phys. Rev.* B **93** 195403
[62] Ormaza M, Robles R, Bachellier N, Abufager P, Lorente N and Limot L 2016 On-surface engineering of a magnetic organometallic nanowire *Nano Lett.* **16** 588
[63] Ormaza M, Abufager P, Verlhac B, Bachellier N, Bocquet M-L, Lorente N and Limot L 2017 Controlled spin switching in a metallocene molecular junction *Nat. Commun.* **8** 1974
[64] Ormaza M *et al* 2017 Efficient spin-flip excitation of a nickelocene molecule *Nano Lett.* **17** 1877
[65] Verlhac B, Bachellier N, Garnier L, Ormaza M, Abufager P, Robles R, Bocquet M-L, Ternes M, Lorente N and Limot L 2019 Atomic-scale spin sensing with a single molecule at the apex of a scanning tunneling microscope *Science* **366** 623
[66] Kögler M, Néel N, Limot L and Kröger J 2024 Structural manipulation of spin excitations in a molecular junction *Nano Lett.* **24** 14355–62
[67] Trishin S, Lotze C, Bogdanoff N, von Oppen F and Franke K J 2021 Moiré tuning of spin excitations: individual Fe atoms on MoS_2/Au(111 *Phys. Rev. Lett.* **127** 236801
[68] Wang Y, Wang B, Huang R, Gao B, Kong F and Zhang Q 2014 First-principles study of transition-metal atoms adsorption on MoS_2 monolayer *Physica* **63E** 276
[69] Chen X, Zhong L, Li X and Qi J 2017 Valley splitting in the transition-metal dichalcogenide monolayer via atom adsorption *Nanoscale* **9** 2188
[70] Moro-Lagares M, Fernández J, Roura-Bas P, Ibarra M R, Aligia A A and Serrate D 2018 Quantifying the leading role of the surface state in the Kondo effect of Co/Ag(111 *Phys. Rev.* B **97** 235442
[71] Blesio G G and Aligia A A 2023 Topological quantum phase transition in individual Fe Atoms on MoS_2/Au(111 *Phys. Rev.* B **108** 045113
[72] Meng X, Möller J, Mansouri M, Sánchez-Portal D, Garcia-Lekue A, Weismann A, Li C, Herges R and Berndt R 2023 Controlling the spin states of FeTBrPP on Au(111) *ACS Nano* **17** 1268
[73] Gao Y, Vlaic S, Gorni T, de' Medici L, Clair S, Roditchev D and Pons S 2023 Manipulation of the magnetic state of a porphyrin-based molecule on gold: from Kondo to quantum nanomagnet via the charge fluctuation regime *ACS Nano* **17** 9082
[74] Xu X, Gao C, Emusani R, Jia C and Xiang D 2024 Toward practical single-molecule/atom switches *Adv. Sci.* **11** 2400877
[75] Xiao X, Chen Z-J, Varley R J and Li C-H 2024 Smart bistable coordination complexes *Smart Mol.* **2** e20230028